다양한 연단조건을 갖는 마름모꼴형 평판의 진동에 대한 모서리 응력특이도의 영향

The Influence of Corner Stress Singularities on the Vibration of Rhombic Plates Having Various Edge Conditions

김 주 우[1] · 정 명 채[2]

Kim, Joo-Woo Cheong, Myung-Chae

요 약 : 본 논문에서는 고정, 단순, 또는 자유 연단 조건의 세 가지의 다른 조합을 갖는 마름모꼴형 평판의 진동에 대한 엄밀한 해석방법을 제시하였다. 본 논문의 주된 관점은 마름모꼴형 평판 둔각모서리에서 형성되는 모멘트특이도를 엄밀히 고려하여 해석하는 것이다. 단 영역 Lagrangian 범함수의 정상조건이 Ritz방법을 이용하여 유도되었다. 진동수의 수렴에 대한 연구는 모서리함수가 수렴속도를 가속화하는 것을 보여주고 있다. 본 논문에서는 모서리 응력특이도의 영향이 이해될 수 있도록 상당히 큰 둔각모서리를 갖는 마름모꼴 형 평판에 대한 정확한 진동수와 수직진동변위의 전형적인 등고선을 제시하였다.

ABSTRACT : An accurate method is presented for vibrations of rhombic plates having three different combinations of clamped, simply supported, and free edge conditions. A specific feature here is that the analysis explicitly considers the moment singularities that occur in the two opposite corners having obtuse angles of the rhombic plates. Stationary conditions of single-field Lagrangian functional are derived using the Ritz method. Convergence studies of frequencies show that the corner functions accelerate the convergence rate of solutions. In this paper, accurate frequencies and normalized contours of the vibratory transverse displacement are presented for highly skewed rhombic plates, so that a significant effect of corner stress singularities may be understood.

핵 심 용 어 : Ritz방법, 진동, 모멘트특이도, 모서리함수, 고유진동수, 모드형상

KEYWORDS : Ritz method, vibration, moment singularities, corner functions, natural frequencies, mode shapes

1) 세명대학교 건축공학과 전임강사, 공학박사

2) 정회원, 전주대학교 건축공학과 조교수, 공학박사

본 논문에 대한 토의를 2001년 2월 28일까지 학회로 보내주시면 토의 회답을 게재하겠습니다.

1. INTRODUCTION

Rhombic plates are used in several practical structures, such as skew bridge or building decks, aircraft wings, ship hulls and vehicle bodies. A considerable quantity of natural frequency data for skew plates has been offered by a number of researchers employing the Ritz, Galerkin, and other approximate procedure. Durvasula[1] used the Galerkin method to determine natural frequencies for clamped skew plates. Mizusawa *et al.*[2] used a Ritz technique with B-spline functions to determine the frequencies of skew plates with a variety of skew angles and boundary conditions. Liew and Lam[3] presented frequencies for skew plates under a variety of edge conditions using the Ritz method with two-dimensional orthogonal plate functions. A Galerkin approach was adopted by Laura and Grosson[4] to determine the upper bound frequencies for a simply supported rhombic plates with a variety of skew angles.

The shortcoming of the various approaches used by the cited researchers is that each has not adequately addressed the unbounded bending stress singularities at a corner having an interior angle larger than 90° (i.e., obtuse). A care must be taken in formulating the approximate procedure in order to avoid erroneous results for rhombic plates having a high degree of skewness. Fundamental stress singularity behavior at obtuse corners in plate flexure problems involving static loads was investigated by Williams[5]. Along these same lines, the importance of considering re-entrant corner stress singularities on the natural vibrations of variously supported rhombic plates has been established in previous work[6,7].

This paper presents a continuing investigation into the influence of corner stress singularities on the flexural vibration of rhombic plates having three different combinations of clamped, simply supported, and free edge conditions. Here, the bending stress singularities that exist at the two of the four interior corners are taken into account explicitly. A Ritz procedure is employed in which the dynamical energy functional is constructed from classical plate theory. The assumed transverse displacement functions consist of a mathematically complete set of algebraic polynomials and two admissible sets of corner functions. The latter functions account for the singular behavior of bending moments at the two corners having obtuse angles. The main objective of this follow-up investigation is to present accurate non-dimensional frequencies and mode shapes, specifically for highly skewed plates, for which no accurate results are previously available.

2. METHOD OF ANALYSIS

Shown in Fig. 1 is a rhombic plate having typical length, c, and diagonal half-lengths, a and b, measured along the Cartesian axes, x and y, respectively. The vibratory transverse displacement of the rhombic plate is $w = w(x, y, t)$, where t is time. For

free vibrations, the temporal dependence of the transverse displacement w is assumed to oscillate cosinusoidally:

$$w(x, y, t) = W(x, y)\cos\omega t \tag{1}$$

where ω is the circular frequency of vibration.

Considering this assumption one can obtain the maximum strain energy V_{max} due to bending a vibratory cycle:

$$V_{max} = \frac{D}{2}\int_A [(\chi_x + \chi_y)^2 - 2(1-\nu)(\chi_x\chi_y - \chi_{xy}^2)]dA, \tag{2}$$

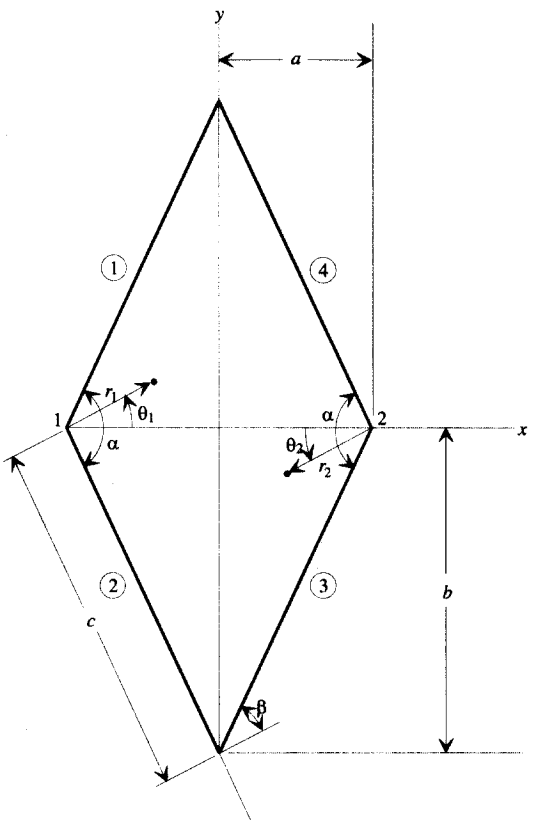

Fig. 1 Geometry of rhombic plates

where $dA = dxdy$, $D = Eh^3/12(1-\nu^2)$ is the flexural rigidity, h is the plate thickness (not shown in Fig. 1), E is Young's modulus, ν is Poisson's ratio, and χ_x, χ_y, and χ_{xy} are the maximum bending and twisting curvatures:

$$\chi_x = \frac{\partial^2 W}{\partial x^2}, \quad \chi_y = \frac{\partial^2 W}{\partial y^2}, \quad \chi_{xy} = \frac{\partial^2 W}{\partial x \partial y} \tag{2a}$$

Similarly, the maximum kinetic energy is

$$T_{max} = \frac{\rho\omega^2}{2}\int_A W^2 dA, \tag{3}$$

where ρ is the mass per unit area of the plate.

In the present Ritz approach, displacement trial functions are assumed as

$$W(x, y) = W_p(x, y) + W_{c_1}(x, y) + W_{c_2}(x, y), \tag{4}$$

where W_p is an admissible and mathematically complete set of algebraic polynomials, and W_{c_1} and W_{c_2} are two sets of corner functions, which account for the singular bending stress behavior at the obtuse corners 1 and 2, respectively (see Fig. 1). It should be noted that simply supported-free (*S-F*), simply supported-simply supported (*S-S*), and clamped-free (*C-F*) edges have singular bending stresses when the included angle (α) formed by the two edges at corners 1 and 2 is larger than approximately 90° (i.e., obtuse)[8]. No such

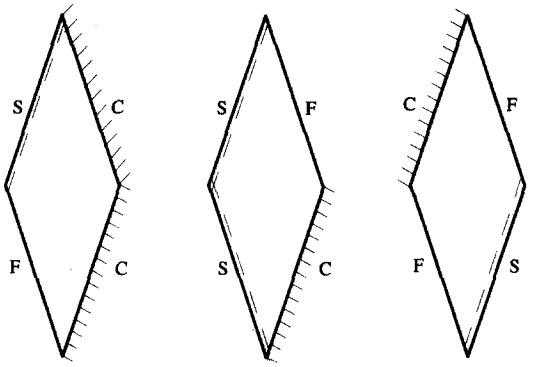

Fig. 2 Rhombic plates with various edge conditions

unbounded stress exists clamped-clamped obtuse for $\alpha \leq 180^{o}$[8].

Three combinations of rhombic plate edge conditions are examined, which are hereafter described as *SFCC*, *SSCF*, and *CFSF*, (see Fig. 2, whereby only those edges which are free have been identified by the letter *F*). These edge conditions are identified according to the numbered edges shown in Fig. 1 (e.g., *S-F-C-C* corresponding to edges 1-2-3-4 as shown).

Let G_j correspond to the equation of the j^{th} edge of the rhombic plate shown in Fig. 1. Thus,

$$G_1 = b - y + \frac{b}{a}x, \quad G_2 = b + y + \frac{b}{a}x,$$
$$G_3 = b + y - \frac{b}{a}x, \quad G_4 = b - y - \frac{b}{a}x. \tag{5}$$

The polynomials W_p are assumed as:

$$SFCC \text{ plate} : W_p(x,y) = G_1 G_3^2 G_4^2 \phi \tag{6a}$$
$$SSCF \text{ plate} : W_p(x,y) = G_1 G_2 G_3^2 \phi, \tag{6b}$$
$$CFSF \text{ plate} : W_p(x,y) = G_1^2 G_3 \phi, \tag{6c}$$

where

$$\phi = \sum_{m}^{M}\sum_{n}^{N} A_{mn} x^m y^n, \tag{6d}$$

and A_{mn} are undetermined coefficients, m, $n = 0, 1, 2, \cdots$, and W_p satisfies the vanishing displacement and normal slope conditions on all the clamped boundaries as required. The corner functions W_{c_i} ($i = 1, 2$) may be written as

$$SFCC \text{ plate} : W_{c_1}(x,y) = G_3^2 G_4^2 \xi_{1_k},$$
$$W_{c_2}(x,y) = 0, \tag{7a}$$

$$SSCF \text{ plate} : W_{c_1}(x,y) = G_3^2 \xi_{1_k}$$
$$W_{c_2}(x,y) = G_1 G_2 \xi_{2_k}, \tag{7b}$$

$$CFSF \text{ plate} : W_{c_1}(x,y) = G_3 \xi_{1_k},$$
$$W_{c_2}(x,y) = G_1^2 \xi_{2_k} \tag{7c}$$

where

$$\xi_{i_k} = \sum_{k=1}^{K} B_{i_k} W^*_{c_{i_k}}(x,y), \tag{7d}$$

in which B_{i_k} are arbitrary coefficients, and $W^*_{c_{i_k}}$ are biharmonic functions, which satisfy the *S-F*, and *S-S*, and *C-F* boundary conditions along two radial edges of a sector plate domain[8]. W_{c_2} is zero for the second of Eq. (7a) because clamped-clamped corners no stress singularities for $\alpha \leq 180^{o}$[8]. For all of the plate edge conditions, $W^*_{c_{i_k}}$ is the k^{th} function of the set:

SFCC plates :

$$W^*_{c_{1_k}}(r_1,\theta_1)=r_1^{\lambda_k+1}[\ \sin(\lambda_k+1)\theta_1 - h_{1_k}\cos(\lambda_k+1)\theta_1 - h_{2_k}\sin(\lambda_k-1)\theta_1 + h_{3_k}\cos(\lambda_k-1)\theta_1], \tag{8a}$$

with

$$h_{1_k}=\frac{\sin(\lambda_k+1)\alpha/2}{\cos(\lambda_k+1)\alpha/2},\quad h_{2_k}=\frac{\eta_k\sin(\lambda_k+1)\alpha/2}{\sin(\lambda_k-1)\alpha/2},\quad h_{3_k}=\frac{\eta_k\sin(\lambda_k+1)\alpha/2}{\cos(\lambda_k-1)\alpha/2}, \tag{8b}$$

where

$$\eta_k=\frac{(\lambda_k+1)(\nu-1)}{\lambda_k(\nu-1)+(3+\nu)}; \tag{8c}$$

SSCF plates :

$$W^*_{c_{1_k}}(r_1,\theta_1)=\begin{cases} r_1^{\lambda_k+1}\cos(\lambda_k+1)\theta_1, & \lambda_k=(2k-1)\pi/\alpha-1 \\ r_1^{\lambda_k+1}\cos(\lambda_k-1)\theta_1, & \lambda_k=(2k-1)\pi/\alpha-1 \\ r_1^{\lambda_k+1}\sin(\lambda_k+1)\theta_1, & \lambda_k=2k\pi/\alpha-1 \\ r_1^{\lambda_k+1}\sin(\lambda_k-1)\theta_1, & \lambda_k=2k\pi/\alpha-1, \end{cases} \tag{9a}$$

$$W^*_{c_{2_k}}(r_2,\theta_2)=r_2^{\lambda_k+1}\ [\sin(\lambda_k+1)\theta_2 + g_{1_k}\cos(\lambda_k+1)\theta_2 + g_{2_k}\sin(\lambda_k-1)\theta_2 + g_{3_k}\cos(\lambda_k-1)\theta_2], \tag{9b}$$

with

$$g_{1_k}=\frac{\mu_{1_k}}{\delta_k},\quad g_{2_k}=\frac{\mu_{2_k}}{\delta_k},\quad g_{3_k}=\frac{\mu_{3_k}}{\delta_k}, \tag{9c}$$

$$\mu_{1_k}=(\lambda_k-1)\gamma_{2_k}\sin(\lambda_k+1)\frac{\alpha}{2} - (\lambda_k+1)\gamma_{1_k}\cos(\lambda_k+1)\frac{\alpha}{2}\sin(\lambda_k-1)\alpha + (\lambda_k-1)\gamma_{1_k}\sin(\lambda_k+1)\frac{\alpha}{2}\cos(\lambda_k-1)\alpha, \tag{9d}$$

$$\mu_{2_k}=(\lambda_k+1)\Big[\gamma_{1_k}\cos(\lambda_k-1)\frac{\alpha}{2} - \gamma_{2_k}\cos(\lambda_k-1)\frac{\alpha}{2}\cos(\lambda_k+1)\alpha - \gamma_{3_k}\sin(\lambda_k-1)\frac{\alpha}{2}\sin(\lambda_k+1)\alpha\Big], \tag{9e}$$

$$\mu_{3_k}=(\lambda_k+1)\Big[\ \gamma_{1_k}\sin(\lambda_k-1)\frac{\alpha}{2} + \gamma_{2_k}\sin(\lambda_k-1)\frac{\alpha}{2}\cos(\lambda_k+1)\alpha - \gamma_{3_k}\cos(\lambda_k-1)\frac{\alpha}{2}\sin(\lambda_k+1)\alpha\Big], \tag{9f}$$

$$\delta_k=(\lambda_k-1)\gamma_{2_k}\cos(\lambda_k+1)\frac{\alpha}{2} - (\lambda_{k+1})\gamma_{1_k}\sin(\lambda_k+1)\frac{\alpha}{2}\sin(\lambda_k-1)\alpha - (\lambda_k-1)\gamma_{1_k}\cos(\lambda_k+1)\frac{\alpha}{2}\cos(\lambda_k-1)\alpha, \tag{9g}$$

in which

$$\gamma_{1_k}=\lambda_k(\nu-1)+(3+\nu),\quad \gamma_{2_k}=(\lambda_k+1)(\nu-1),\quad \gamma_{3_k}=(\lambda_k-1)(\nu-1); \tag{9h}$$

CFSF plates :

$$W^*_{c_{1_k}}(r_1,\theta_1)=r_1^{\lambda_k+1}[\ \sin(\lambda_k+1)\theta_1 + g_{1_k}\cos(\lambda_k+1)\theta_1 + g_{2_k}\sin(\lambda_k-1)\theta_1 + g_{3_k}\cos(\lambda_k-1)\theta_1], \tag{10a}$$

$$W^*_{c_{2_k}}(r_2,\theta_1)=r_2^{\lambda_k+1}[\ \sin(\lambda_k+1)\theta_2 - h_{1_k}\cos(\lambda_k+1)\theta_2 - h_{2_k}\sin(\lambda_k-1)\theta_2 + h_{3_k}\cos(\lambda_{k-1})\theta_2], \tag{10b}$$

with Eqs. (8b), (8c), and (9c)-(9h) for h_{l_k} and g_{l_k} (l = 1, 2, 3). In the above Eqs. (8)-(10), the local polar coordinates (r_i, θ_i) originate at corners 1 and 2 (Fig. 1), and α is the included angle of corners 1 and 2.

In Eq. (9a) (i.e., *S*-*S* edge), the λ_k are so defined, whereas in Eqs (8), (9b)-(9h), and (10), the λ_k are the roots of the character equation:

C-*F* boundary condition:

$$\sin^2\lambda_k\alpha=\frac{4}{(1-\nu)(3+\nu)-\frac{1-\nu}{3+\nu}\lambda_k^2\sin^2\alpha}, \tag{11}$$

S-*F* boundary condition:

$$\sin 2\lambda_k\alpha=\frac{\nu-1}{3+\nu}\lambda_k\sin 2\alpha. \tag{12}$$

Recall that the corner functions $W^*_{c_{i_k}}$ are expressed in terms of the local polar coordinates (r_i, θ_i). These functions are then transformed to the global Cartesian coordinates (x, y) through the following relations:

$$r_1=[(x+a)^2+y^2]^{1/2},\quad \theta_1=\tan^{-1}[y(x+a)^{-1}], \tag{13a}$$

$$r_2=[(x-a)^2+y^2]^{1/2},\quad \theta_2=\tan^{-1}[y(x-a)^{-1}] \tag{13b}$$

The Ritz minimizing equations are formulated by substituting Eqs. (4)-(10) and (13) into (2) and (3) and taking the partial derivatives:

$$\frac{\partial}{\partial A_{mn}}(V_{\max}-T_{\max})=0,\quad \frac{\partial}{\partial B_{i_k}}(V_{\max}-T_{\max})=0 \tag{14}$$

This results in a set of linear homogeneous algebraic equations involving the constants A_{mn} and B_{i_k}. The vanishing determinant of these equations yields a set of eigenvalues (i.e., natural frequencies), expressed in terms of the non-dimensional frequency parameter $\omega a^2\sqrt{\rho/D}$, which is particularly suitable for the rhombic plate. The associated eigenvalue problem is positive definite, and thus the frequency and mode shape data has been obtained by using QL algorithm combined Cholesky factorization[9,10].

Eigenvectors involving the coefficients A_{mn} and B_{i_k} may be determined in the usual manner by substituting the eigen-

values back into the homogeneous equations. Normalized contours of the associated mode shapes may be depicted on a x-y grid in the rhombic plate domain once the eigenvectors are substituted into Eqs. (6d) and (7d).

3. CONVERGENCE STUDIES AND MODE SHAPES

Table 1 summarizes a convergence study for the first six non-dimensional frequencies $\omega a^2\sqrt{\rho/D}$ of *SSCF* rhombic plates having

Table 1. Convergence of frequency parameters $\omega a^2\sqrt{\rho/D}$ for SSCF rhombic plate ($b/a=3$)

Mode No.	Corner Functions (W_c)	(M+1)×(N+1) polynomial terms (W_p)						
		8×8	9×9	10×10	11×11	12×12	13×13	14×14
1	0	2.5368	2.5029	2.4888	2.4719	2.4652	2.4561	2.4526
	4	2.4309	2.4295	2.4293	2.4289	2.4289	2.4288	2.4287
	8	2.4297	2.4290	2.4290	2.4288	2.4288	2.4287	2.4287
	12	2.4289	2.4287	2.4287	2.4287	2.4287	2.4287	---
	16	2.4288	2.4287	2.4287*	---	---	---	---
2	0	5.6447	5.6145	5.6094	5.5921	5.5885	5.5775	5.5747
	4	5.5011	5.4990	5.4981	5.4977	5.4976	5.4975	5.4975
	8	5.4986	5.4979	5.4976	5.4975	5.4975	5.4974	5.4974
	12	5.4977	5.4975	5.4974	5.4974	5.4974	5.4974	---
	16	5.4975	5.4974	5.4974*	---	---	---	---
3	0	8.1916	8.1112	8.0587	8.0398	8.0069	7.9987	7.9764
	4	7.9386	7.8868	7.8837	7.8794	7.8789	7.8785	7.8784
	8	7.9300	7.8835	7.8822	7.8786	7.8785	7.8782	7.8782
	12	7.8856	7.8791	7.8788	7.8782	7.8782	7.8782	---
	16	7.8813	7.8789	7.8778*	---	---	---	---
4	0	11.705	11.633	11.512	11.496	11.470	11.463	11.451
	4	11.524	11.482	11.421	11.417	11.411	11.410	11.410
	8	11.502	11.464	11.419	11.415	11.410	11.410	11.410
	12	11.477	11.436	11.416	11.413	11.410	11.410	---
	16	11.419	11.414	11.411*	---	---	---	---
5	0	12.885	12.769	12.631	12.576	12.530	12.506	12.482
	4	12.562	12.518	12.424	12.410	12.406	12.403	
	8	12.523	12.490	12.419	12.408	12.404	12.403	12.403
	12	12.495	12.454	12.408	12.406	12.402	12.402	---
	16	12.418	12.410	12.404*	---	---	---	---
6	0	17.471	16.495	16.377	16.052	16.033	15.998	15.992
	4	17.166	16.397	16.281	15.980	15.969	15.937	15.936
	8	17.097	16.362	16.273	15.977	15.968	15.937	15.936
	12	16.386	16.122	16.060	15.958	15.950	15.936	---
	16	16.238	16.084	15.967*	---	---	---	---

*singular value decomposition eigenanalysis
--- no results due to matrix ill-conditioning

$b/a=3$ (or $\alpha \cong 143°$). In all calculations, the Poisson's ratio (ν) has been set to 0.3. Use of the corner functions W_c in conjunction with the polynomials W_p permits one to represent to properly the corner stress singularities in rhombic plate vibrations. The $(M+1)\times(N+1)$ number of polynomial terms (W_p) shown in Table 1 indicate $M+1$ terms retained in the x-direction and $N+1$ terms retained in the y-direction [see Eqs. (6)]. The $2K$ number of corner functions ($W_c = W_{c_1} + W_{c_2}$) define K corner functions used in Eqs. (7) for each of corners 1 and 2.

For large solution determinant sizes, however, the mass operator used in a QL reduction algorithm may become ill-conditioned, causing some eigenvalue extraction algorithm to abort. Hence, the data marked with a superscript asterisk (*) in Table 1 were obtained by using an algorithm based upon two numerical techniques. These are: (i) a Householder reduction of the dynamical matrices to bidiagonal from with matrix diagonalization achieved by using a QL procedure with shift[9,10] and (ii) a singular value decomposition technique[11] using a threshold (matrix conditioning) number of 10^{-25}.

Close scrutiny of the frequency data in Table 1 shows that by using polynomial terms alone typically results in slow convertgence of upper bound $\omega a^2\sqrt{\rho/D}$ values. However, the convergence rate of $\omega a^2\sqrt{\rho/D}$ is considerably accelerated when a few corner functions are added to the polynomials. This is mainly attributed to the influence of vibratory bending stress singularities at the obtuse corners 1 and 2 (Fig. 1), which are examined more closely below. For example, using 100 polynomial terms (10×10) without corner functions to represent the fundamental (lowest frequency) mode of an *SSCF* plate with $b/a=3$ (see Table 1) yields an error of approximately 2.4% in the predicted frequncy. Increasing to 196 polynomial terms (14×14) still results in an error of 1.0%. When the trial set of 100 polynomials are supplemented with 4 corner functions the predicted frequency error reduces to a negligible amount of 0.02%. A similar level of solution accuracy may be seen in all mode of the *SSCF* (Table 1) and the other boundary condition cases (i.e., *SFCC* and *CFSF* plates, which are not shown here for brevity).

Depicted in Fig. 3 are the vibratory transverse displacement contours corresponding to the least upper bound frequency data for the first six modes listed for *SFCC*, *SSCF*, and *CFSF*. The displacement contours in Fig. 3 are normalized with respect to the maximum displacement component (i.e., $-1 \le W/W_{max} \le 1$, where the negative values of W/W_{max} are depicted as dashed contour lines in Figs 3a and 3b). Non- dimensional frequencies $\omega a^2\sqrt{\rho/D}$ shown in Fig. 3 correspond to the con- verged values. Nodal patterns of each mode are shown in Fig. 3 as slightly darker contour lines of zero displacement $W/W_{max}=0$ during vibratory motion.

Case	Mode Number					
	1	2	3	4	5	6
SFCC		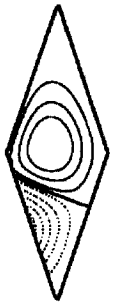	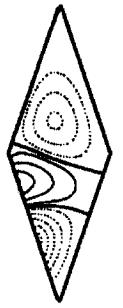	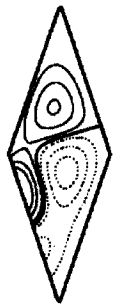	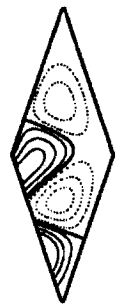	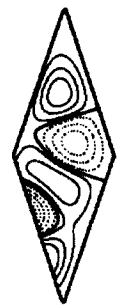
	4.1090	6.7808	10.108	13.036	14.815	18.417
SSCF	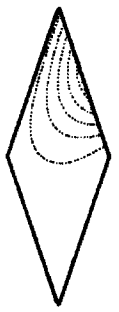	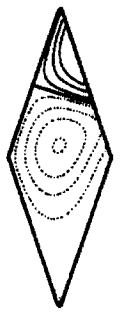	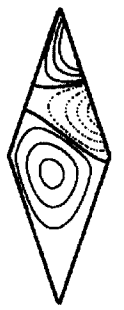	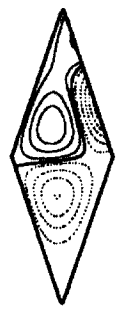		
	2.4287	5.4974	7.8782	11.410	12.402	15.936
CFSF	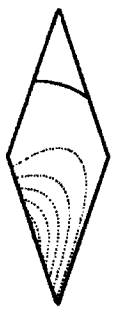	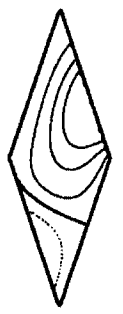	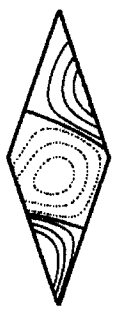	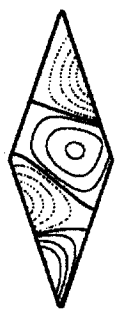		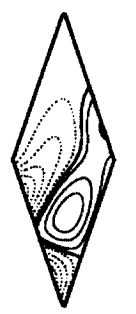
	2.4245	4.0517	5.7480	7.9417	10.713	12.130

Fig. 3 Normalized transverse displacement contours (W/W_{max}) for the first six modes of SFCC, SSCF and CFSF rhombic plates ($b/a=3$)

4. FREQUENCY RESULTS

Table 2 shows a summary of accurate frequencies for *SFCC*, *SSCF*, and *CFSF* rhombic plates having skew angles β (corner angles α) = 15°(105°), 30°(120°), 45°(135°), 60°(150°), and 75°(165°). Listed therein are the first five non-dimensional frequencies $\omega c^2\sqrt{\rho/D}$ (c being the side length, as shown in Fig. 1). Accurate qualitative modeling of the singular stress phenomena dictates that for large $\beta(\alpha)$, a considerable number of corner functions are required at corners 1 and 2 for the *SSCF* and *CFSF* rhombic plates, and at corner 1 for the *SFCC* plates. Sufficient numbers of polynomials (W_p) and corner functions (W_c) were used to yield at least five significant digits accuracy of the frequencies shown in Table 2, whereby the converged solution sizes employed are summarized in Table 3.

It may be seen in Table 2 that as the side length c remains constant $\omega c^2\sqrt{\rho/D}$ increases with increasing β, and that the

Table 2. Frequency parameters $\omega a^2\sqrt{\rho/D}$ for rhombic plate

Skew Angle(β)	α	c/a	Mode No.	SFCC	SSCF	CFSF
0°	90°	1.000	1	17.540 (17.615)+	16.792* (16.865)	15.195 (15.285)
			2	36.025 (36.064)	31.113* (31.138)	20.591 (20.673)
			3	51.818 (52.065)	51.394* (51.631)	39.741 (39.775)
			4	71.082 (71.194)	64.020* (64.043)	49.458 (49.730)
			5	74.327 (74.349)	67.537* (67.646)	56.296 (56.617)
15°	105°	1.303	1	19.219	16.842	15.848
			2	37.688	31.742	21.336
			3	56.032	53.467	40.242
			4	69.688	62.584	52.116
			5	83.180	74.186	59.670
30°	120°	1.732	1	23.326	18.302	17.850
			2	42.560	35.426	24.231
			3	68.326	59.456	42.693
			4	74.499	68.225	59.883
			5	102.44	91.197	70.914
45°	135°	2.414	1	32.183	21.455*	21.348
			2	54.425	45.094*	31.948
			3	85.668	68.621*	49.764
			4	100.82	90.426*	70.450
			5	125.68	109.90*	90.931
60°	150°	3.732	1	53.306	27.829	27.800
			2	87.978	66.813	52.715
			3	123.06	95.559	67.622
			4	165.94	138.65	93.350
			5	187.31	151.52	124.55
75°	165°	7.596	1	134.84	46.496	46.453
			2	221.22	113.90	113.79
			3	196.63	193.36	134.73
			4	358.72	270.74	192.40
			5	445.66	328.85	221.12

*singular value decomposition eigenanalysis
+Results in paranthesis cf Leissa12)

Table 3. Number of polynomial and corner function terms required of the five significant figure frequency convergence of Table 2

Edges	β (degrees)	Polynomial terms	Corner function
SFCC	0	12×12	0
	15, 30	12×12	2
	45	12×12	4
	60	14×14	8
	75	16×16	8
SSCF	0, 15, 30	12×12	4
	45	12×12	8
	60	14×14	8
	75	16×16	12
CFSF	0	12×12	0
	15, 30	12×12	4
	45	12×12	8
	60	14×14	12
	75	16×16	16

highest frequency values are obtained for the *SFCC* plates, which is to be expected. For all plates, substantial changes in $\omega c^2\sqrt{\rho/D}$ traceable to plate skewness are most distinguishable for $45^\circ \leq \beta \leq 75^\circ$, where one can observe increasingly greater frequency changes as the mode number increases. Frequency solutions for the square plates ($\alpha = 90^\circ$, $\beta = 0^\circ$) are lower upper-bound $\omega c^2\sqrt{\rho/D}$ values compared to those values reported in reference [12], which were obtained by employing the Ritz method with beam eigenfunction approximations of the plate's normal displacement.

5. CONCLUDING REMARKS

This paper presents the first known solutions for free vibrations of classically thin, skewed *SFCC*, *SSCF*, *CFCF* rhombic plates, in which stress singularities explicitly include at the two obtuse corners. The dynamical energies of the plate have been extremized using the Ritz method with the transverse displacement field approximated by mathematically complete polynomials and admissible corner functions that account for the unbounded stresses at the obtuse corners.

The feasibility of the assumed hybrid displacement field has been demonstrated by means of a convergence table. It is shown that poor convergence of frequencies is typically obtained when only polynomial displacement trial functions are used, and that upper bound convergence of solution improves significantly when the hybrid trial sets of polynomials and corner functions are simultaneously utilized. The accurate frequencies and mode shapes for highly skewed ($\beta > 45^\circ$) rhombic plates have been offered here for comparison with future data obtained by other investigators.

REFERENCES

(1) Durvasula, S., Natural Frequencies and Modes of Clamped Skew Plates, *American Institute of Aeronautics and Asternautics Journal*, Vol. 7, pp. 1164-1166, 1969.

(2) Mizusawa, T., Kajita, T., and Naruoka, M., Vibration of Skew Plates Using B-spline Functions, *Journal of Sound and Vibration*, Vol. 62, pp. 301-308, 1979.

(3) Liew, K. M. and Lam, K. Y., Application of two-dimensional Orthogonal Plate Function to Flexural Vibrations of Skew Plates, *Journal of Sound and Vibration*, Vol. 139, pp. 241-252, 1990.

(4) Laura, P. A. and Grosson, J., Fundamental Frequency of Vibration of Rhombic Plates, *Journal of Acoustical Society of America*, Vol. 44, pp. 823-824, 1968.

(5) Williams, M. L., Surface stress singularities resulting from various boundary conditions in angular corners of plates under bending, *Proceedings of the first U.S. National Congress of Applied Mechanics*, pp. 325-329, 1951.

(6) McGee, O. G., Kim, J. W., and Leissa, A. W., The Influence of Corner Stress Singularities on the Vibration Characteristics of Rhombic Plates with Combinations of Simply Supported and Free Edges, *International Journal of Mechanical Sciences*, Vol. 41, No. 1, pp. 17-41, 1999.

(7) Kim, J. W. and Han, B. H., Accurate Vibration of Rhombic Plates with Various Combinations of Edge Conditions Considering Corner Stress Singularities, *Journal of the Computational Structural Engineering Institute of Korea*, Vol. 11, No. 4. pp. 275-285, 1998.

(8) Leissa, A. W., McGee, O. G., and Huang, C. S., Vibration of sectorial plates having corner stress singularities, *Journal of Applied Mechanics*, Vol. 60, pp. 134-140, 1993.

(9) Stewart, G. W., *Introduction to Matrix Computation*, New York: Academic Press, 1970.

(10) Stoer, J. and Bulirsh, R., *Introduction to Numerical Analysis*, New York: Springer-Verlag, 1980.

(11) Press, W. H., Flannery, B. P., Teukolsky, S. A., and Vetterling, W. T., *Numerical Recipes-the Art of Scientific Computing*, Cambridge: Cambridge University Press, 1986.

(12) Leissa, A. W., The free vibration of rectangular plates, *Journal of Sound and Vibration* Vol. 31, 1971, pp. 257-293.

(접수일자 : 2000년 3월 14일)